An Intramolecularly Base-Stabilized Diphosphagermylene and Two Unusual Germanium(II) Ate Complexes: A Structural, NMR, and DFT Study

Keith Izod,* William McFarlane, Ben Allen, William Clegg, and Ross W. Harrington

Department of Chemistry, School of Natural Sciences, Bedson Building, University of Newcastle, Newcastle upon Tyne, NE1 7RU, U.K.

Received February 17, 2005

The reaction between $GeCl_2$·dioxane and 1 equiv of $\{R(C_6H_4\text{-}2\text{-}CH_2NMe_2)P\}K$ (**5**) yields the heteroleptic complex $\{R(C_6H_4\text{-}2\text{-}CH_2NMe_2)P\}GeCl$ (**6**) [R = $(Me_3Si)_2CH$]. Treatment of GeI_2 with 2 equiv of the potassium salt **5** gives the homoleptic, intramolecularly base-stabilized diphosphagermylene $\{R(C_6H_4\text{-}2\text{-}CH_2NMe_2)P\}_2Ge$ (**7**) in good yield. In contrast, treatment of GeI_2 with 2 equiv of $\{R(C_6H_4\text{-}2\text{-}CH_2NMe_2)P\}Li$ (**4**) in ether reproducibly yields the unusual ate complex $\{R(C_6H_4\text{-}2\text{-}CH_2NMe_2)P\}_2GeLi_2I_2(OEt_2)_3$ (**8**), whereas treatment of GeI_2 or $GeCl_2$·dioxane with 3 equiv of **5** yields the cage ate complex $\{R(C_6H_4\text{-}2\text{-}CH_2NMe_2)P\}_3GeK$ (**9**). The solid-state structures of **7**−**9** have been determined by X-ray crystallography, and the dynamic behavior of **6**−**9** in solution has been studied by multielement and variable-temperature NMR experiments. DFT calculations on the model complex $\{(Me)(C_6H_4\text{-}2\text{-}CH_2NMe_2)P\}GeCl$ (**6a**) indicate that inversion at germanium via a planar transition state is disfavored [E_{inv} = 38.5 kcal mol^{-1}] with respect to inversion at phosphorus [E_{inv} = 21.0 kcal mol^{-1}]; inversion at germanium is calculated to proceed via an edge-inversion rather than vertex-inversion process. For the model diphosphagermylene $\{(Me)(C_6H_4\text{-}2\text{-}CH_2NMe_2)P\}_2Ge$ (**7a**) the lowest energy process for epimerization is calculated to be inversion at germanium via a pseudo-trigonal bipyramidal intermediate [E_{inv} = 3.0 kcal mol^{-1}]. Inversion at germanium (via a vertex-inversion process) is calculated to have a barrier of 48.0 kcal mol^{-1}, whereas the barriers to inversion at phosphorus are 24.0 and 18.5 kcal mol^{-1} for the chelating and terminal phosphorus atoms, respectively.

Introduction

Diaminocarbenes $(R_2N)_2C$: and their heterocyclic analogues, the *N*-heterocyclic carbenes (NHCs), have been widely studied since Arduengo and co-workers first isolated stable examples of these compounds in 1991.[1−3] The stability of diaminocarbenes is ascribed to efficient overlap of the heteroatom lone pairs with the vacant carbene p_π orbital, mitigating the electron deficiency at this center and stabilizing the singlet relative to the triplet state of the carbene; because of this $n-p_\pi$ overlap, diaminocarbenes are highly nucleophilic but only very weakly electrophilic.[2,4] The weaker $n-p_\pi$ overlap in diphosphinocarbenes and -silylenes, $(R_2P)_2E$: (E = C, Si) results in significantly reduced stability,[5] and consistent with this, isolable phosphinocarbenes are largely limited to the so-called "push−pull" phosphinosilyl- and phosphinophosphonio-carbenes, $(R_2P)(R_3Si)C$: and $[(R_2P)(R_3P)C:]^+$, respectively,[2,6] although Bertrand and co-workers have recently reported a range of moderately stable aryl- and alkyl-substituted phosphinocarbenes, $(R_2P)ArC$: [Ar = e.g., 2,4,6-$Me_3C_6H_2$].[7] Le Floch and co-workers have also reported a zirconocene complex of a phosphorus analogue of an Arduengo-type carbene, although the free carbene has not been isolated.[8]

Whereas the chemistry of stable diaminocarbenes and their silicon analogues has emerged only recently, the corresponding diaminogermylenes $(R_2N)_2Ge$ have been known since the 1970s,[9−11] principally because of the comparative ease with which germanium(II) species may be accessed from the readily available starting

* To whom correspondence should be addressed. E-mail: k.j.izod@ncl.ac.uk.

(1) Arduengo, A. J., III; Harlow, R. L.; Kline, M. *J. Am. Chem. Soc.* **1991**, *113*, 361.

(2) For recent reviews of stable carbenes see: (a) Krimse, W. *Angew. Chem., Int. Ed.* **2004**, *43*, 1767. (b) Bourissou, D.; Guerret, O.; Gabbai, F. P.; Bertrand, G. *Chem. Rev.* **2000**, *100*, 39. (c) Arduengo, A. J., III. *Acc. Chem. Res.* **1999**, *32*, 913. (d) Hermann, W. A. *Angew. Chem., Int. Ed.* **2002**, *41*, 1291.

(3) For recent reviews of stable silylenes see: (a) Gehrhus, B.; Lappert, M. F. *J. Organomet. Chem.* **2001**, *617−618*, 209. (b) Haaf, M.; Schmedake, T. A.; West, R. *Acc. Chem. Res.* **2000**, *33*, 704. (c) Tokitoh, N.; Okazaki, R. *Coord. Chem. Rev.* **2000**, *210*, 251.

(4) For examples see: (a) Gillette, G. R.; Noren, G. H.; West, R. *Organometallics* **1989**, *8*, 487. (b) Kira, M.; Ishida, S.; Iwamoto, T.; Yauchibara, R.; Sakurai, H. *J. Organomet. Chem.* **2001**, *636*, 144.

(5) Fekete, A.; Nyulaszi, L. *J. Organomet. Chem.* **2002**, *643−644*, 278.

(6) Buron, C.; Gornitzka, H.; Romanenko, V.; Bertrand, G. *Science* **2000**, *288*, 834.

(7) (a) Despagnet, E.; Gornitzka, H.; Rozhenko, A. B.; Schoeller, W. W.; Bourissou, D.; Bertrand, G. *Angew. Chem., Int. Ed.* **2002**, *41*, 2835. (b) Despagnet-Ayoub, E.; Sole, S.; Gornitzka, H.; Rozhenko, A. B.; Schoeller, W. W.; Bourissou, D.; Bertrand, G. *J. Am. Chem. Soc.* **2003**, *125*, 124. (c) Despagnet, E.; Miqueu, K.; Gornitzka, H.; Dyer, P. W.; Bourissou, D.; Bertrand, G. *J. Am. Chem. Soc.* **2002**, *124*, 11834. (d) Lavallo, V.; Mafhouz, J.; Canac, Y.; Donnadieu, B.; Schoeller, W. W.; Bertrand, G. *J. Am. Chem. Soc.* **2004**, 126, 8670.

(8) Cantat, T.; Mezailles, N.; Maigrot, N.; Ricard, L.; Le Floch, P. *Chem. Commun.* **2004**, 1274.

10.1021/om0501125 CCC: $30.25
Publication on Web 03/31/2005

Scheme 1[a]

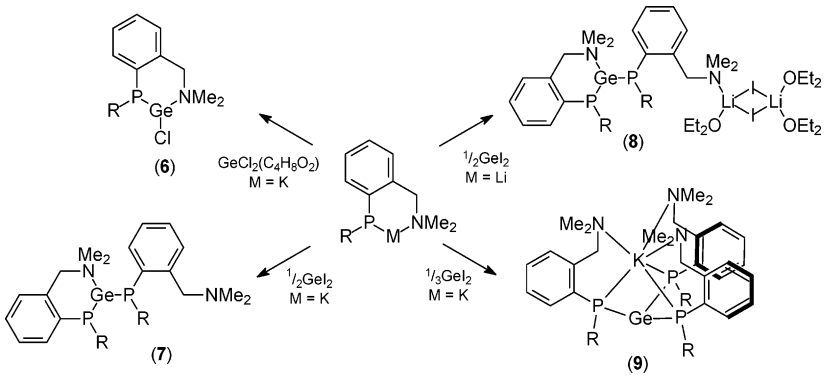

[a] R = $(Me_3Si)_2CH$.

materials GeI_2 and $GeCl_2$(1,4-dioxane). However, while diaminogermylenes and related compounds with good π-donor substituents, e.g., dialkoxygermylenes $(RO)_2Ge$, are well known,[10] the corresponding diphosphagermylenes $(R_2P)_2Ge$, in which P−Ge n−p_π interactions are likely to be rather weak, are less well established.[12,13] Crystallographically characterized germanium(II) phosphides are limited to just three examples: the dimeric compounds $\{(t\text{-}Bu_2P)GeCl\}_2$ (**1**)[12] and $\{(i\text{-}Pr_2P)_2Ge\}_2$ (**2**)[12] and the monomeric compound $[\{(Tripp)_2FSi\}(i\text{-}Pr_3Si)P]_2Ge$ (**3**) [Tripp = 2,4,6-i-$Pr_3C_6H_2$].[13] Although compound **3** is the only reported example of a true diphosphagermylene species, structural data on this compound were too poor for detailed analysis. In addition to these germanium(II) phosphides, Karsch and co-workers have reported the synthesis and structural characterization of several formally Ge(I) and Ge(II) derivatives supported by P-donor diphosphinomethanide ligands.[14]

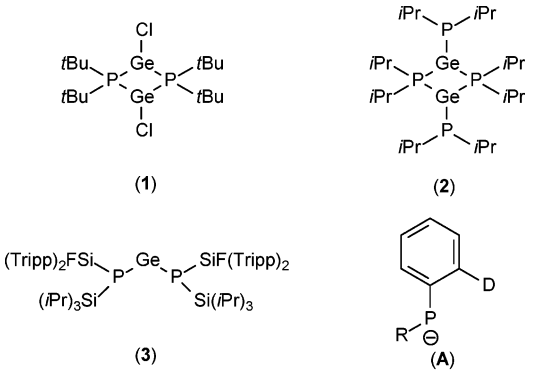

As part of an ongoing investigation into the chemistry of sterically demanding, donor-functionalized phosphides (**A**), we have recently reported complexes of these ligands with a variety of metals from groups 1 and 2 and the lanthanides.[15] We now report the synthesis of several novel germanium(II) complexes with one of these ligands, including an intramolecularly base-stabilized diphosphagermylene and two unusual *ate* complexes, their solid-state structures, and their dynamic behavior in solution.

Results and Discussion

Metathesis reactions between the alkali metal salts $[\{(Me_3Si)_2CH\}P(C_6H_4\text{-}2\text{-}CH_2NMe_2)]M$ [M = Li (**4**), K (**5**)][15a] and either $GeCl_2$(dioxane) or GeI_2 are highly sensitive to the reaction stoichiometry and the nature of the alkali metal starting materials. The reaction between $GeCl_2$(dioxane) and 1 equiv of **5** in THF gives the heteroleptic complex $[\{(Me_3Si)_2CH\}P(C_6H_4\text{-}2\text{-}CH_2NMe_2)]GeCl$ (**6**) in good yield (Scheme 1). Compound **6**, which is soluble in hydrocarbon solvents, was identified by its ^1H and $^{31}P\{^1H\}$ NMR spectra (see below) and elemental analysis; despite repeated attempts, crystals suitable for X-ray crystallography could not be obtained.

Treatment of GeI_2 or $GeCl_2$(dioxane) with slightly less than 2 equiv of the potassium salt **5** in THF gives the intramolecularly base-stabilized diphosphagermylene $[\{(Me_3Si)_2CH\}P(C_6H_4\text{-}2\text{-}CH_2NMe_2)]_2Ge$ (**7**) as orange-yellow, hydrocarbon-soluble crystals in excellent yield (Scheme 1). The ^1H and $^{31}P\{^1H\}$ NMR spectra of **7** are extremely broad at room temperature due to dynamic exchange processes (see below); however, the composition of **7** was established unequivocally by X-ray crystallography and elemental analysis.

Single crystals of **7** were obtained by recrystallization from cold (−30 °C) hexamethyldisiloxane/DME [DME

(9) (a) Davidson, P. J.; Harris, D. H.; Lappert, M. F. *J. Chem. Soc., Dalton Trans.* **1976**, 2268. (b) Gynane, M. J. S.; Harris, D. H.; Lappert, M. F.; Power, P. P. Riviere, P.; Riviere-Baudet, M. *J. Chem. Soc., Dalton Trans.* **1977**, 2004.

(10) For a recent review see: Barrau, J.; Rima, G. *Coord. Chem. Rev.* **1998**, *178*−*180*, 593.

(11) For a recent review of *N*-heterocyclic germylenes see: Kuhl, O. *Coord. Chem. Rev.* **2004**, *248*, 411.

(12) Druckenbrodt, C.; du Mont, W.-W.; Ruthe, F.; Jones, P. G. *Z. Anorg. Allg. Chem.* **1998**, *624*, 590.

(13) Driess, M.; Janoschek, R.; Pritzkow, H.; Rell, S.; Winkler, U. *Angew. Chem., Int. Ed. Engl.* **1995**, *34*, 1614.

(14) (a) Karsch, H. H.; Appelt, A.; Hanika, G. *J. Organomet. Chem.* **1986**, *312*, C1. (b) Karsch, H. H.; Deubelly, B.; Hanika, G.; Riede, J.; Müller, G. *J. Organomet. Chem.* **1988**, *344*, 153. (c) Karsch, H. H.; Deubelly, B.; Riede, J. Müller, G. *Angew. Chem., Int. Ed. Engl.* **1987**, *26*, 673. (d) Karsch, H. H.; Deubelly, B.; Riede, J.; Müller, G. *J. Organomet. Chem.* **1987**, *336*, C37. (e) Karsch, H. H.; Hofmann, J.; Müller, G. *Chem. Commun.* **1988**, 516. (f) Karsch, H. H.; Baumgartner, G.; Gamper, S. *J. Organomet. Chem.* **1993**, *462*, C3. (g) Schoeller, W. W.; Sundermann, A. Reiher, M.; Rozhenko, A. *Eur. J. Inorg. Chem.* **1999**, 1155.

(15) (a) Clegg, W.; Doherty, S.; Izod, K.; Kagerer, H.; O'Shaughnessy, P.; Sheffield, J. M. *J. Chem. Soc., Dalton Trans.* **1999**, 1825. (b) Blair, S.; Izod, K.; Harrington, R. W.; Clegg, W. *Organometallics* **2003**, *22*, 302. (c) Blair, S.; Izod, K.; Clegg. W. *Inorg. Chem.* **2002**, *41*, 3886. (d) Blair, S.; Izod, K.; Clegg, W.; Harrington, R. W. *Eur. J. Inorg. Chem.* **2003**, *18*, 3319. (e) Clegg, W.; Izod, K.; Liddle, S. T.; O'Shaughnessy, P.; Sheffield, J. M. *Organometallics* **2000**, *19*, 2090. (f) Izod, K.; O'Shaughnessy, P.; Sheffield, J. M.; Clegg, W.; Liddle, S. T. *Inorg. Chem.* **2000**, *39*, 4741. (g) Clegg, W.; Izod, K.; Liddle, S. T. *J. Organomet. Chem.* **2000**, *613*, 128. (h) Blair, S.; Izod, K.; Clegg, W. *J. Organomet. Chem.* **2003**, *688*, 92. (i) Izod, K.; Liddle, S. T.; Clegg, W. *Organometallics* **2004**, *23*, 2734.

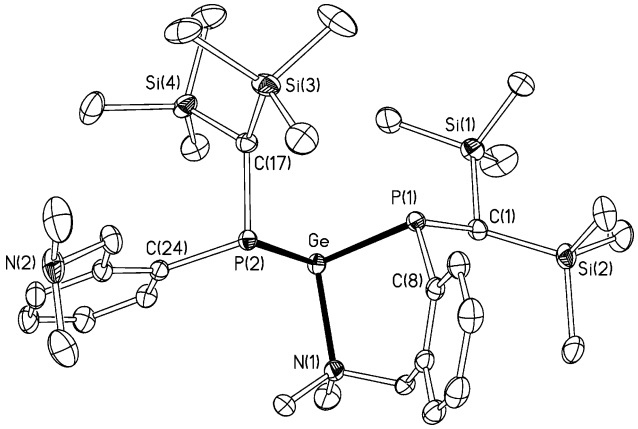

Figure 1. Molecular structure of **7** with 40% probability ellipsoids. H atoms and disordered solvent of crystallization omitted for clarity. Selected bond lengths (Å) and angles (deg): Ge−P(1) 2.4023(4), Ge−P(2) 2.4114(4), Ge−N(1) 2.1888(13), P(1)−C(1) 1.8855(14), P(1)−C(8) 1.8409(15), P(2)−C(17) 1.8960(15), P(2)−C(24) 1.8576(14), Si(1)−C(1) 1.8965(16), Si(2)−C(1) 1.8980(16), P(1)−Ge-P(2) 89.467(13), P(1)−Ge−N(1) 97.49(3), P(2)−Ge−N(1) 97.98(4), Ge−P(1)−C(1) 102.43(5), Ge−P(1)−C(8) 102.02(5), C(1)−P(1)−C(8) 108.68(7), Ge−P(2)−C(17) 95.60(4), Ge−P(2)−C(24) 106.14(5), C(17)−P(2)−C(24) 105.56(6), P(1)−C(1)−Si(1) 104.44(7), P(1)−C(1)−Si(2) 116.23(8), Si(1)−C(1)−Si(2) 114.13(8), P(2)−C(17)−Si(3) 113.33(8), P(2)−C(17)−Si(4) 120.59(8), Si(3)−C(17)−Si(4) 115.78(8).

= 1,2-dimethoxyethane]. Although the donor solvent DME is not retained, the unit cell of the crystal examined contained half a molecule of disordered methylcyclohexane per molecule of **7**, probably arising from incomplete solvent removal from a previous recrystallization attempt using this solvent. This solvent is not observed in the NMR spectra of a second crop of crystals obtained in the same way, but which had not been exposed to methylcyclohexane and which were not of X-ray quality. The molecular structure of **7** along with selected bond lengths and angles is shown in Figure 1. Compound **7** is chiral at the two phosphorus centers and at the germanium atom and crystallizes as discrete monomers in the space group $P\bar{1}$ as a racemic mixture of the $Ge_S P^{ch}{}_S P^t{}_R$ and $Ge_R P^{ch}{}_R P^t{}_S$ stereoisomers (where P^{ch} and P^t refer to the phosphorus atoms in the chelating and terminal phosphide ligands, respectively).

The germanium center in **7** is bound by the P and N atoms of one phosphide ligand to give a six-membered chelate ring [P−Ge−N bite angle 97.49(3)°] and by the P atom of the other phosphide ligand, giving a three-coordinate, trigonal pyramidal germanium atom with a stereochemically active lone pair [sum of angles at Ge 284.94°]; the remaining nitrogen atom has no short intra- or intermolecular contacts with germanium. The Ge−P distances of 2.4023(4) and 2.4114(4) Å to the chelating and terminal ligands, respectively, are comparable with the Ge−P distances in the previously reported, structurally characterized germanium(II) diphosphide **2** [2.4261(11), 2.4217(11), and 2.3981(11) Å].[12] The Ge−N distance of 2.1888(13) Å in **7** lies in the range of previously reported Ge(II)−N distances; for example, the Ge−N distances in the intramolecularly base-stabilized alkylgermylenes $Ge\{C(SiMe_3)_2(2\text{-}C_5H_4N)\}Cl$[16] and $Ge\{C(SiMe_3)_2(SiMe_2\text{-}2\text{-}C_5H_4N)\}Cl$[17] are 2.082(4) and 2.075(4) Å and 2.0814(16) Å, respectively, and the

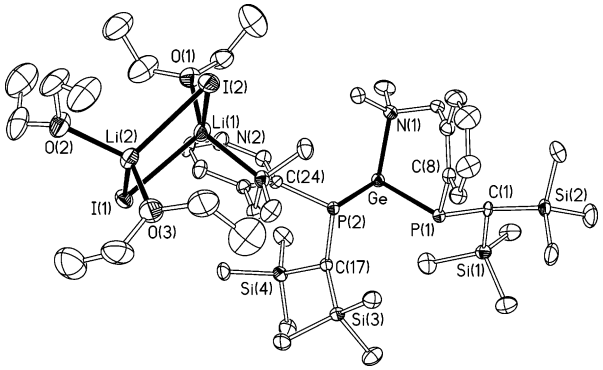

Figure 2. Molecular structure of **8** with 40% probability ellipsoids. H atoms and minor disorder components omitted for clarity. Selected bond lengths (Å) and angles (deg): Ge−P(1) 2.4114(13), Ge−P(2) 2.4106(14), Ge−N(1) 2.183(4), P(1)−C(1) 1.886(5), P(1)−C(8) 1.877(5), P(2)−C(17) 1.909(5), P(2)−C(24) 1.862(5), Si(1)−C(1) 1.892(5), Si(2)−C(1) 1.895(5), N(2)−Li(1) 2.136(10), Li(1)−I(1) 2.786(11), Li(1)−I(2) 2.802(10), Li(1)−O(1) 1.941(11), Li(2)−I(1) 2.760(10), Li(2)−I(2) 2.804(12), Li(2)−O(2) 1.963(10), Li(2)−O(3) 1.980(11), P(1)−Ge−P(2) 83.53(5), P(1)−Ge−N(1) 97.72(12), P(2)−Ge−N(1) 100.54(12), C(1)−P(1)−C(8) 106.3(2), C(1)−P(1)−Ge 106.48(17), C(8)−P(1)−Ge 100.81(15), C(17)−P(2)−C(24) 104.3(2), C(17)−P(2)−Ge 92.72(15), C(24)−P(2)−Ge 108.85(16), P(1)−C(1)−Si(1) 108.1(2), P(1)−C(1)−Si(2) 113.2(3), Si(1)−C(1)−Si(2) 113.8(2), P(2)−C(17)−Si(3) 110.6(2), P(2)−C(17)−Si(4) 121.2(3), Si(3)−C(17)−Si(4) 114.5(3), Li(1)−I(1)−Li(2) 78.9(3), Li(1)−I(2)−Li(2) 77.8(3), I(1)−Li(1)−I(2) 101.3(3), I(1)−Li(2)−I(2) 101.9(4).

Ge−N distance in the germylene-borane adduct $Ge(C_6H_3\text{-}2,6\text{-}NMe_2)_2(BH_3)$ is 2.110(6) Å.[18] The P atoms in both the chelating and terminal ligands are distinctly pyramidal [sum of angles at P(1) 313.13°, P(2) 307.30°], suggesting little $n-p_\pi$ overlap, consistent with intramolecular base stabilization of the germanium(II) center.

Whereas metathesis reactions between GeI_2 and 2 equiv of **5** yield the homoleptic complex **7**, treatment of GeI_2 with 2 equiv of the lithium salt **4** in diethyl ether reproducibly gives pale yellow crystals which give positive test results for both lithium and iodide and which are soluble in ethereal solvents but only sparingly soluble in hydrocarbons. The ^1H and $^{31}P\{^1H\}$ NMR spectra of these crystals in d_8-THF are rather broad due to dynamic exchange processes (see below), but indicate the presence of both phosphide and ether ligands. The identity of the yellow crystals was confirmed unambiguously by X-ray crystallography and elemental analysis as the novel *ate* complex $[\{(Me_3Si)_2CH\}P(C_6H_4\text{-}2\text{-}CH_2\text{-}NMe_2)]_2Ge{\cdot}Li_2I_2(OEt_2)_3$ (**8**) (Scheme 1). Compound **8** thus constitutes an unusual adduct between the diphosphagermylene **7** and the LiI elimination product.

Although crystalline samples of **8** are only sparingly soluble in hydrocarbons, single crystals may be obtained by recrystallization of a freshly prepared sample of **8** from cold (−30 °C) methylcyclohexane. The molecular structure of **8** is shown in Figure 2 along with selected bond lengths and angles.

(16) Benet, S.; Cardin, C. J.; Cardin, D. J.; Constantine, C. P.; Heath, P.; Rashid, H.; Teixeira, S.; Thorpe, J. H.; Todd, A. K. *Organometallics* **1999**, *18*, 389.
(17) Al Juaid, S. S.; Avent, G. A.; Eaborn, C.; Hill, M. S.; Hitchcock, P. B.; Patel, D. J.; Smith, J. D. *Organometallics* **2001**, *20*, 1223.
(18) Drost, C.; Hitchcock, P. B.; Lappert, M. F. *Organometallics* **1998**, *17*, 3838.

As in **7**, the germanium atom is bound by the P and N atoms of one phosphide ligand to give a six-membered chelate ring [P−Ge−N bite angle 97.71(12)°] and by the phosphorus atom of the second phosphide ligand; there is no contact between the germanium center and the remaining N atom. Thus, the germanium atom is three-coordinate, with a stereochemically active lone pair, and adopts a trigonal pyramidal geometry. The Ge−P distances to the chelating and monodentate ligands [2.4114(13) and 2.4106(14) Å, respectively] are similar to those observed in **7**.

Somewhat unexpectedly, the nitrogen atom of the terminal phosphide ligand is bound to a Li_2I_2 fragment generated during the metathesis reaction. The Li−I distances in **8** range from 2.760(10) to 2.804(12) Å and compare with Li−I distances of 2.932(6) and 2.913(7) Å in dimeric $Li_2I_2(2,6\text{-}Me_2C_5H_3N)$[19] and 2.822(6) Å in the heterocubane cluster $[LiI(NEt_3)]_4$.[20]

It is of note that the coordination geometry of the germanium atom in **7** [sum of angles at Ge = 284.94°] is remarkably similar to that of **8** [sum of angles at Ge = 281.79°], indicating that retention of the Li_2I_2 moiety in the latter has little impact on the germanium center itself.

Treatment of either GeI_2 or $GeCl_2$(dioxane) with *slightly more than 2 equiv* of the potassium salt **5** in THF yields a deep red solution. Removal of solvent in vacuo and recrystallization of the red oil from *n*-hexane preferentially yields a small amount of deep red crystals of the unusual ate complex $[\{(Me_3Si)_2CH\}P(C_6H_4\text{-}2\text{-}CH_2\text{-}NMe_2)]_3GeK$ (**9**); compound **9** may be isolated in reasonable yield from the reaction of GeI_2 with 3 equiv of **5**. ^{31}P NMR spectra obtained from a solution of **9** in d_8-THF over the temperature range −85 to +60 °C exhibit two distinct singlets at −53 and −63.9 ppm, which show no evidence of coalescence; these signals may be attributed to **7** and **5**, respectively, indicating that **9** is unstable in donor solvents with respect to decomposition into its constituent parts. However, variable-temperature $^{31}P\{^1H\}$ NMR spectra of **9** in d_8-toluene exhibit a single singlet at −55 ppm, which merely broadens slightly at lower temperatures, suggesting that the integrity of the ate complex is unperturbed by nondonor solvents. The room-temperature ^1H NMR spectrum of **9** in d_8-toluene is consistent with the solid-state structure (see below) and exhibits a single set of phosphide ligand signals: the Me_3Si groups give rise to two well-separated singlets at 0.24 and 0.96 ppm, and the diastereotopic benzylic protons give rise to two well-separated doublets at 3.05 and 5.08 ppm ($^2J_{HH}$ = 11.3 Hz).

The molecular structure of **9** is shown in Figure 3 along with selected bond lengths and angles. Compound **9** crystallizes as discrete molecules having exact crystallographic C_3 symmetry; compound **9** is chiral at each of the phosphorus atoms and crystallizes as a racemic mixture of $P_RP_RP_R$ and $P_SP_SP_S$ enantiomers. The germanium atom is coordinated by three phosphorus atoms in a trigonal pyramidal arrangement [sum of angles at Ge 286.98°]; the stereochemically active lone pair is oriented away from the molecule along the C_3 axis. The potassium atom is bound by both the P and N atoms of each of the three phosphide ligands, forming three six-membered chelate rings and enforcing an essentially trigonal antiprismatic geometry on the potassium atom. Thus, the three phosphorus atoms bridge the germanium and potassium centers, forming an unusual cage cluster. The Ge−P distance of 2.4570(7) Å in **9** is significantly longer than the same distances in **7** and **8**, but is similar to the Ge−P distances in **1**;[12] the P−K distance of 3.2141(10) Å is similar to the P−K distance [3.2323(6) Å] in the potassium derivative of this ligand $[\{(Me_3Si)_2CH\}P(C_6H_4\text{-}2\text{-}CH_2NMe_2)]K$(pmdeta) (**10**) [pmdeta = *N*,*N*,*N*′,*N*″,*N*″-pentamethyldiethylenetriamine].[15a] Similarly, the P−K−N bite angle of the ligand in **9** [74.47(5)°] is comparable to that in **10** [75.53(3)°].

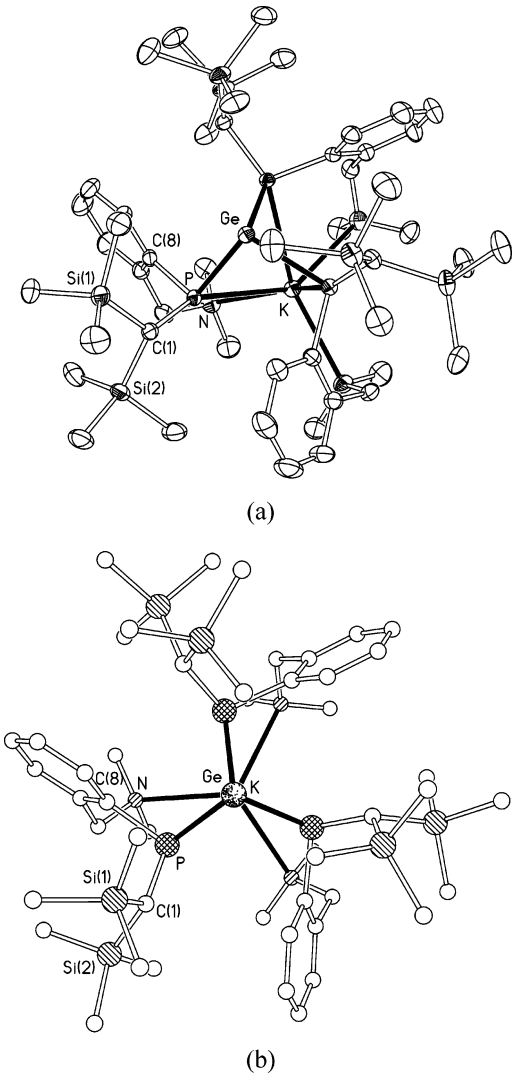

Figure 3. (a) Molecular structure of **9** with 40% probability ellipsoids and with H atoms omitted for clarity. (b) View of **9** along the 3-fold symmetric Ge−K axis. Selected bond lengths (Å) and angles (deg); the primed atoms are related to unprimed atoms by a 3-fold rotation axis about the Ge···K vector: Ge···K 3.7019(11), Ge−P 2.4570(7), K−P 3.2141(10), K−N 2.897(3), Si(1)−C(1) 1.903(3), Si(2)−C(1) 1.903(3), P−C(1), 1.887(3), P−C(8) 1.855(3), P−Ge−P′ 95.66(2), P−K−P′ 69.02(3), P−K−N 74.47(5), N−K−N′ 109.76(5), Ge−P−K 80.29(2), Ge−P−C(1) 102.03(9), Ge−P−C(8) 105.80(9), K−P−C(1) 153.58(9), K−P−C(8) 100.42(9), C(1)−P−C(8) 104.11(12).

(19) Raston, C. L.; Whitaker, C. R.; White, A. H. *Inorg. Chem.* **1989**, *28*, 163.

(20) Doriat, C.; Köppe, R.; Baum, E.; Stösser, G.; Köhnlein, H.; Schnöckel, H. *Inorg. Chem.* **2000**, *39*, 1534.

Scheme 2[a]

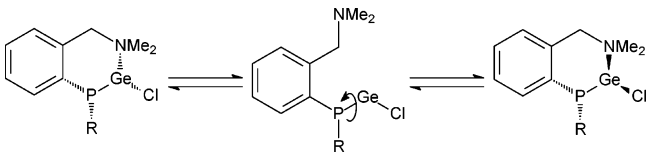

[a] R = $CH(SiMe_3)_2$.

Reactions between GeI_2 or $GeCl_2$(dioxane) and either 3 equiv of **4** or of the sodium analogue [{$(Me_3Si)_2CH$}-$P(C_6H_4$-2-$CH_2NMe_2)$]Na gave red solutions, possibly containing the ate complexes [{$(Me_3Si)_2CH$}$P(C_6H_4$-2-$CH_2NMe_2)]_3GeM$ [M = Li, Na]; however, we were unable to obtain any solid products from these reactions.

Dynamic Behavior of 6−9. Compound **6** is chiral at both the P and Ge centers and is highly fluxional in solution. $^{31}P\{^1H\}$ NMR spectra of **6** in d_8-toluene exhibit a singlet at −34.9 ppm over the temperature range 80−45 °C, this singlet becoming significantly broadened as the temperature decreases. As the temperature is reduced to ambient, this signal decoalesces into two broad resonances at −46.4 and −34.8 ppm, and these signals sharpen further as the temperature is lowered until, at −80 °C, the spectrum consists of two relatively sharp singlets at −47.9 and −34.3 ppm in an approximately 4:1 ratio. The ^1H NMR spectra of **6** also change significantly with temperature: at 40 °C and above the diastereotopic $(SiMe_3)_2$, NMe_2, and benzylic CH_2 groups each give rise to two well-resolved resonances. As the temperature is lowered, these signals broaden substantially; below room temperature they begin to sharpen again as a new set of ligand signals begins to appear. At −80 °C the spectrum contains two distinct sets of signals due to the phosphide ligands in an approximately 3:1 ratio. These spectra are consistent with the presence of two distinct diastereomers at low temperatures, with one diastereomer significantly favored over the other; these diastereomers are in rapid equilibrium above room temperature.

Interconversion of the two diastereomers may proceed via any of three mechanisms: (i) inversion at phosphorus, (ii) inversion at the germanium center via a planar transition state, or (iii) inversion at germanium via Ge−N cleavage/Ge−P rotation/Ge−N re-coordination (Scheme 2).

To our knowledge, there has been no detailed study of the inversion of trigonal pyramidal germanium(II) species; compound **6**, by virtue of its diastereomeric nature and the ease with which inversion processes may be monitored using ^{31}P NMR spectroscopy, provides a unique opportunity to gain some insight into these processes.

Pyramidal, three-coordinate germanium(II) compounds are isoelectronic with the corresponding triorganoarsine species R_3As. The barrier to inversion in triorganopnictogen compounds increases significantly on descending the group, and inversion at trigonal pyramidal phosphorus is usually slow on the NMR time scale; inversion at trigonal pyramidal arsenic is typically significantly slower [the inversion barriers for NH_3, PH_3, and AsH_3 have been calculated as 6, 36, and 46 kcal mol^{-1}, respectively].[21] This suggests that epimerization

(21) Dixon, D. A.; Marynick, D. S. *J. Am. Chem. Soc.* **1977**, *99*, 6101.

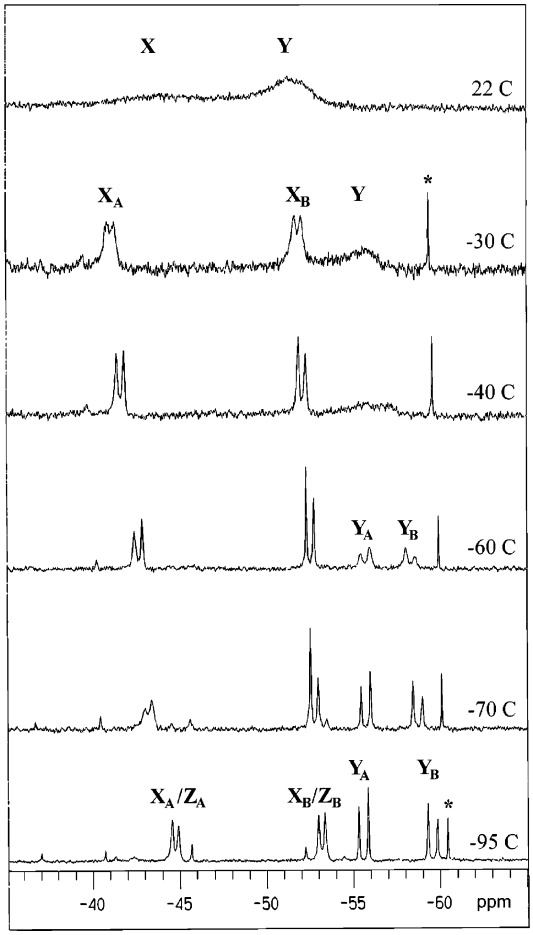

Figure 4. $^{31}P\{^1H\}$ NMR spectra of **7** in d_8-toluene at various temperatures. Asterisk denotes a persistent impurity.

of **6** through inversion at germanium via a planar transition state is unlikely. However, it is not possible to attribute the observed epimerization to one or other of the two remaining inversion processes on NMR evidence alone. To gain further insight into the dynamic processes affecting **6**, we undertook a preliminary DFT study of the model compound [MeP(C_6H_4-2-CH_2NMe_2)]-GeCl (**6a**); the results of these calculations are described below.

Compound **7** is also subject to dynamic exchange processes in solution. The three chiral centers in **7** (the phosphorus atoms of the terminal and chelating ligands and the germanium center) potentially give rise to four pairs of diastereomers; in the solid-state structure only the $Ge_SP^{ch}{}_SP^t{}_R$ diastereomer and its enantiomer are observed. At 90 °C the ^1H NMR spectrum of **7** in d_8-toluene exhibits singlets for the diastereotopic $(SiMe_3)_2$, NMe_2, and benzylic CH_2 groups along with four broad multiplets in the aromatic region, consistent with rapid inversion at all stereocenters in the molecule. At lower temperatures the ^1H spectra become increasingly complicated, with many broad, overlapping signals which are impossible to assign, but which are consistent with the presence of several species in solution.

The room-temperature $^{31}P\{^1H\}$ NMR spectrum of **7** in the same solvent consists of two extremely broad, overlapping signals centered at approximately −44 and −51 ppm (Figure 4, **X** and **Y**, respectively). As the temperature is raised, these signals coalesce to give a

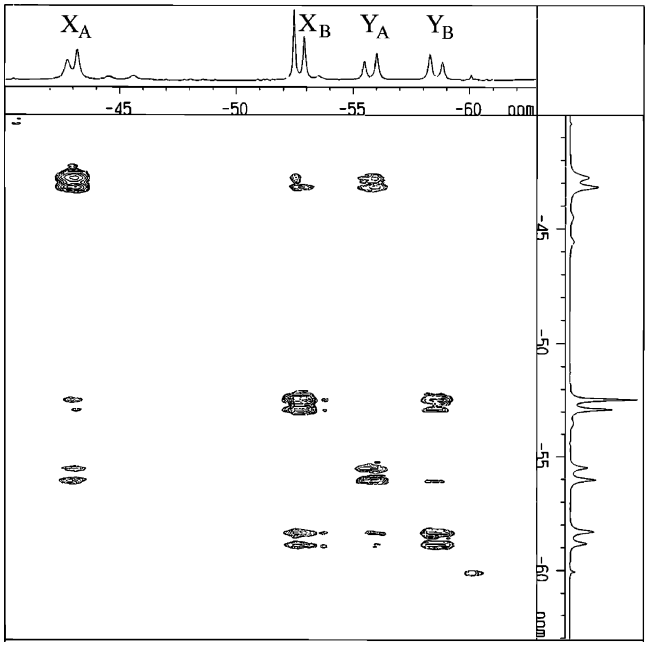

Figure 5. ^{31}P EXSY spectrum of **7** in d_8-toluene at −66 °C.

single signal, which sharpens until, at 90 °C, the spectrum consists of a sharp singlet at −45.8 ppm. As the temperature is reduced below ambient, the two signals observed at room temperature begin to decoalesce further, but at different rates; at −30 °C the low-field signal **X** has decoalesced to a fairly well-resolved pair of doublets $\mathbf{X_A}$ and $\mathbf{X_B}$, whereas the high-field signal **Y** remains a very broad singlet. At −40 °C the high-field signal begins to decoalesce and by −60 °C the spectrum consists of two pairs of well-resolved doublets at −52.6 and −42.7 ppm ($\mathbf{X_A}$ and $\mathbf{X_B}$, respectively; $^2J_{PP}$ = 86.8 Hz) and −58.3 and −55.8 ppm ($\mathbf{Y_A}$ and $\mathbf{Y_B}$, respectively; $^2J_{PP}$ = 113.5 Hz) in an approximately 2:1 ratio. As the temperature is lowered further, the high-field pair of signals $\mathbf{Y_A/Y_B}$ sharpens while the low-field pair of signals $\mathbf{X_A/X_B}$ begins to broaden until, at −70 °C, a new pair of doublets $\mathbf{Z_A/Z_B}$ begins to appear. At the lowest temperature we were able to attain (−95 °C) the spectrum consists of a well-resolved pair of doublets at −59.4 and −55.6 ppm ($^2J_{PP}$ = 109.1 Hz) and two overlapping pairs of doublets at −53.1 and −44.4 ppm ($^2J_{PP}$ = 67.0 Hz) and −53.0 and −45.1 ($^2J_{PP}$ = 215 Hz) with approximate relative intensities **Y**:**X**:**Z** of 4:5:1.

These spectra are consistent with the presence of two major and one minor diastereomer (**X**, **Y**, and **Z**, respectively) at low temperatures that are in rapid equilibrium at higher temperatures. A ^{31}P EXSY spectrum of **7** in d_8-toluene obtained at −66 °C (Figure 5) shows that the following exchange processes are rapid: $\mathbf{X_A} \leftrightarrow \mathbf{Y_A}$, $\mathbf{X_B} \leftrightarrow \mathbf{Y_B}$, and $\mathbf{X_A} \leftrightarrow \mathbf{X_B}$, where the subscripts indicate the type of phosphorus atom in a particular diastereomer (i.e., chelating or terminal); however, the process $\mathbf{Y_A} \leftrightarrow \mathbf{Y_B}$ is slow on the NMR time scale. Exchange processes involving the minor diastereomer **Z** were not detected owing to its low concentration at this temperature.

In addition to the three epimerization pathways (i−iii, above) available to **6**, compound **7** may undergo epimerization via Ge−N_a dissociation (to give transition state **II**, Scheme 3) followed by Ge−N_b coordination. This process interconverts P_a and P_b between chelating and terminal binding modes and, if the sense of the chelate ring involving P_b is opposite that involving P_a, results in inversion at germanium (process c in Scheme 3). If it is assumed that the relative positions of the ^{31}P signals due to the chelating and terminal phosphide ligands in each diastereomer are always consistent (i.e., that the low-field signal $\mathbf{X_A/Y_A}$ in each diastereomer may always be attributed to the chelating ligand and the high-field signal $\mathbf{X_B/Y_B}$ to the terminal ligand, or vice versa) and that inversion at the germanium center via a planar transition state is again slow on the NMR time scale (see discussion of **6** above), then the major observed exchange processes ($\mathbf{X_A} \leftrightarrow \mathbf{Y_A}$ and $\mathbf{X_B} \leftrightarrow \mathbf{Y_B}$) will not involve interconversion of the chelating and terminal ligands within a diastereomer. These processes may thus be attributed either to inversion at one or other of the phosphorus centers or to inversion at germanium via Ge−N_a cleavage/Ge−P_a rotation/Ge−N_a re-coordination (process b in Scheme 3) and this process must be rapid on the NMR time scale. It is not possible to assign this epimerization process unambiguously to any of these pathways or to distinguish between inversion at either the chelating or the terminal phosphorus atom

Scheme 3. Dynamic Exchange in 7 via (a) Inversion at Phosphorus (inversion at the terminal phosphorus shown), (b) Inversion at Germanium via Ge−N_a Cleavage/Ge−P_a Rotation/Ge−N_a Re-coordination, (c) Inversion at Germanium and Simultaneous Exchange of the Terminal and Chelating Phosphorus Atoms via Ge−N_a Cleavage/Ge−N_b Coordination, and (d) Exchange of the Chelating and Terminal Phosphorus Atoms *without* Inversion at Germanium or Phosphorus (i.e., N_a/N_b exchange)[a]

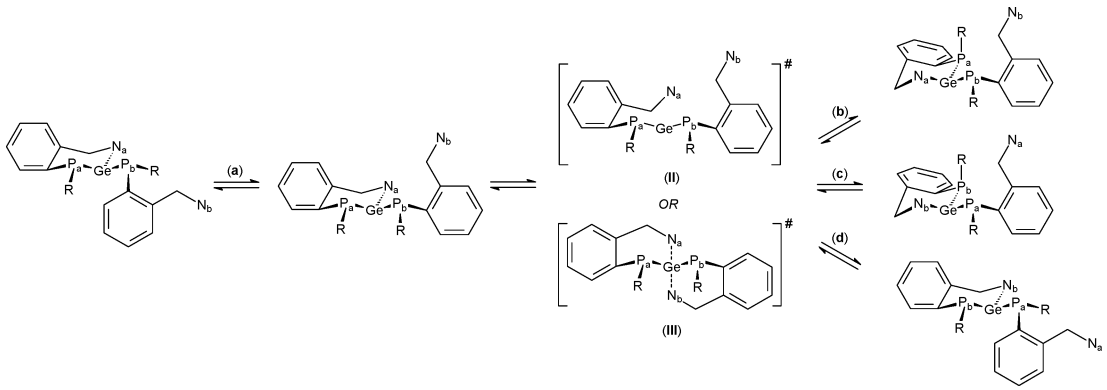

[a] Processes c and d may proceed via a dissociative (**II**) or associative (**III**) pathway.

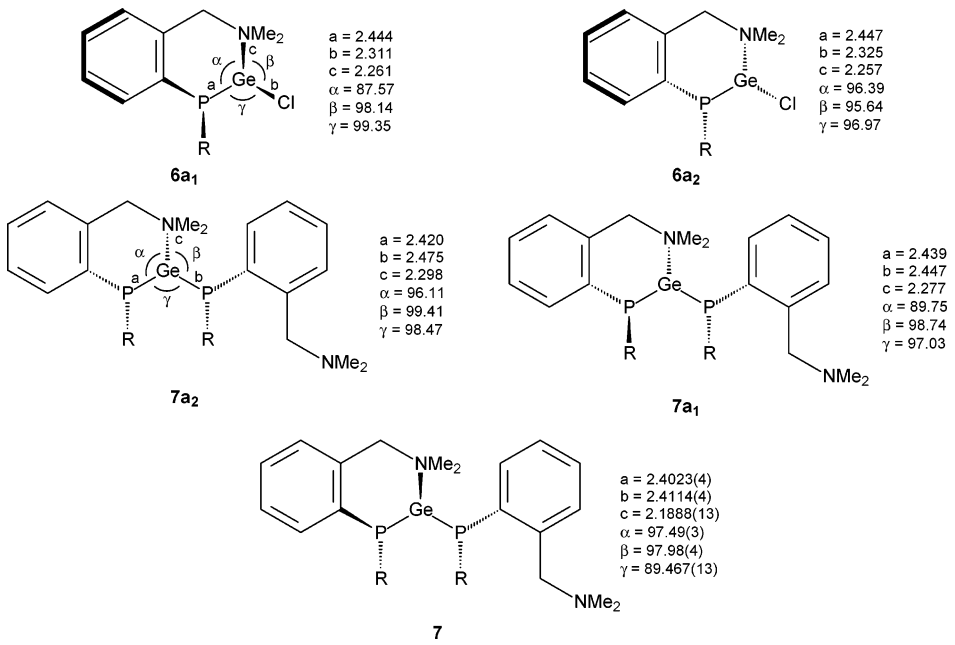

Figure 6. Structures of the calculated minima for **6a** and **7a** and comparison with the X-ray structure of **7** [bond lengths in Å, angles in deg].

in each diastereomer; however, inversion of the phosphorus atom in the chelating ligand would require significant conformational changes in the chelate ring and so is likely to be disfavored with respect to inversion at the terminal phosphorus ligand.

Exchange between the chelating and terminal ligands (i.e., $\mathbf{X_A} \leftrightarrow \mathbf{X_B}$ or $\mathbf{Y_A} \leftrightarrow \mathbf{Y_B}$; process d in Scheme 3) *without inversion at germanium* (i.e., via $Ge-N_a$ cleavage/$Ge-N_b$ coordination to give a chelate ring involving N_b with the same sense as that involving N_a in the starting diastereomer) is highly dependent on the nature of the diastereomer itself: for diastereomer **X** this exchange is fairly rapid at −66 °C, whereas for diastereomer **Y** it is slow on the NMR time scale at this temperature. In both cases this exchange process appears to be slower than the epimerization processes. An alternative, associative mechanism is also plausible for processes c and d; this would proceed via a pseudotrigonal bipyramidal transition state in which the amino substituents of both ligands are associated with the germanium center (**III**).

Compound **8** is only sparingly soluble in toluene, and so all NMR spectra were recorded in d_8-THF. In this solvent the variable-temperature $^{31}P\{^1H\}$ NMR spectra of **8** are remarkably similar to those of **7**. The marked similarity between the NMR spectra of **7** in toluene and **8** in THF suggests that in THF solution the Li_2I_2 fragment dissociates from **8** and that the resulting diphosphagermylene moiety is subject to the same dynamic processes in THF as in toluene.

The NMR spectra of **9** have already been described; these suggest that in d_8-THF dissociation to **5** and **7** occurs, but that in d_8-toluene compound **9** retains its cage structure.

DFT Calculations. To gain further insight into the dynamic processes affecting **6** and **7**, we have undertaken a preliminary DFT study of the model compounds [{(Me)(C_6H_4-2-CH_2NMe_2)P}GeCl] (**6a**) and [{(Me)(C_6H_4-2-CH_2NMe_2)P}$_2$Ge] (**7a**), in which the bulky bis(trimethylsilyl)methyl groups of **6** and **7** have been replaced by sterically unencumbered methyl groups, to save on computational resources. Although this necessarily introduces an underestimate of the steric compression at both the germanium and phosphorus centers and a commensurate underestimate of the effect of steric influences on the dynamic behavior of **6** and **7**, the basic framework of these compounds is preserved and so it is still possible to draw meaningful conclusions regarding the dynamic processes affecting these two compounds from their models.

Initial optimized geometries of **6a** and **7a** were obtained using the B3LYP hybrid functional[22] with an SKJBC effective core potential basis set for all atoms.[23] Subsequently, the geometries of the minima and transition states obtained for **6a** and **7a** were reoptimized using an all-electron 6-311G* basis set on the core Ge, N, and P atoms and a 3-21G* basis set on the C and H atoms.[24] Optimized geometries for both global minima and transition states were very similar for calculations using either the ECP or all-electron basis sets, and so, for simplicity, we discuss below only the results from the latter calculations.

The key bond lengths and angles calculated for **6a** and **7a** are shown graphically in Figure 6 alongside the corresponding parameters obtained for **7** by X-ray crystallography. The calculations reveal two minima for **6a**, corresponding to two different chelate ring conformations of the Ge_RP_S diastereomer and its enantiomer; in conformer $\mathbf{6a_1}$ the aromatic ring of the ligand is on the same side of the chelate ring as the P-Me and Cl groups, whereas in $\mathbf{6a_2}$ (the Ge_SP_R enantiomeric form

(22) (a) Becke A. D. *J. Chem. Phys.* **1993**, *98*, 5648. (b) Stephens, P. J.; Devlin, F. J.; Chablowski, C. F.; Frisch, M. J. *J. Phys. Chem.* **1994**, *98*, 11623. (c) Hertwig, R. H.; Koch, W. *Chem. Phys. Lett.* **1997**, *268*, 345.

(23) (a) Stevens, W. J.; Basch, H.; Krauss, M. *J. Chem. Phys.* **1984**, *81*, 6026. (b) Stevens, W. J.; Krauss, M.; Basch, H.; Jasien, P. G. *Can. J. Chem.* **1992**, *70*, 612. (c) Cundari, T. R.; Stevens, W. J. *J. Chem. Phys.* **1993**, *98*, 5555.

(24) Krishnan, R.; Binkley, J. S.; Seeger, R.; Pople, J. A. *J. Chem. Phys.* **1980**, *72*, 650.

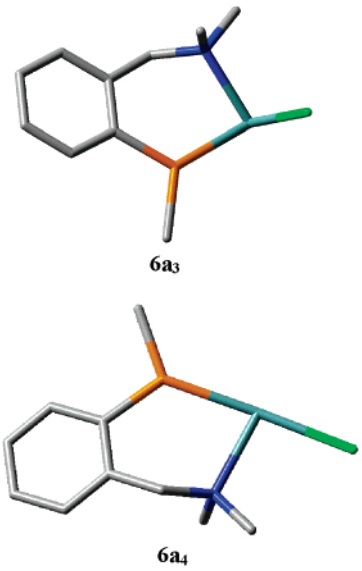

Figure 7. Transition states for inversion at phosphorus (**6a$_3$**) and edge inversion at germanium (**6a$_4$**).

of **6a$_1$**) the aromatic ring is oriented toward the opposite side of the chelate ring to these substituents. Conformer **6a$_1$** is 2.5 kcal mol^{-1} more stable than conformer **6a$_2$**.

Calculations also reveal two accessible minima for **7a**, which correspond to epimers at the chelating phosphorus atom; **7a$_1$** corresponds to the Ge$_R$P$^{ch}{}_S$P$^t{}_S$ stereoisomer, while **7a$_2$** corresponds to the Ge$_R$P$^{ch}{}_R$P$^t{}_S$ stereoisomer. Stereoisomer **7a$_1$** is calculated to be 6.5 kcal mol^{-1} more stable than **7a$_2$**.

The gross structural features found by X-ray crystallography for **7** are replicated quite well in the calculated structures of the model compounds **7a$_1$** and **7a$_2$**. In both cases the minimum energy structures consist of a trigonal pyramidal germanium atom coordinated by the P and N atoms of one phosphide ligand and the P atom of a second phosphide ligand; there is no contact between germanium and the second nitrogen atom. The calculated bond lengths for the core Ge, N, and P atoms in **7a$_1$** and **7a$_2$** are approximately 0.02−0.10 Å longer than the corresponding distances in the X-ray crystal structure of **7**; the angles around the P and Ge atoms in **7a$_1$** and **7a$_2$** also deviate somewhat from the corresponding angles in **7**, although this is likely an artifact of the smaller size of the methyl substituents in **7a** when compared to the (Me$_3$Si)$_2$CH groups in **7**. The calculated Ge−P^{ch} and Ge−P^t bond lengths are 2.439 and 2.447 Å (**7a$_1$**) and 2.420 and 2.457 Å (**7a$_2$**) [cf. 2.4023(4) and 2.4114(4) Å, respectively, in **7**], while the P−Ge−N bite angles of **7a$_1$** and **7a$_2$** are 89.75° and 96.11°, respectively [cf. 97.49(3)° in **7**]. The pyramidal nature of the Ge atoms is reflected in the sums of the angles at this center [sum of angles at Ge: 285.52° (**7a$_1$**), 294.39° (**7a$_2$**), 284.94° (**7**)], as is the pyramidal nature of the phosphorus atom in the chelating ligand [sum of angles at P^{ch}: 295.73° (**7a$_1$**), 311.25° (**7a$_2$**), 313.13° (**7**)] and in the terminal ligand [sum of angles at P^t: 293.41° (**7a$_1$**), 290.71° (**7a$_2$**), 307.30° (**7**)].

Transition states were located for epimerization of the lower energy conformer **6a$_1$** at both the phosphorus and germanium centers (Figure 7). We were unable to locate a transition state for inversion at phosphorus or germanium involving a two-coordinate germanium center

Scheme 4. Edge Inversion of a Trigonal Pyramidal Compound E(a)(b)(c) Showing the Vacant p-Type Orbital in the T-Shaped Transition State[27b]

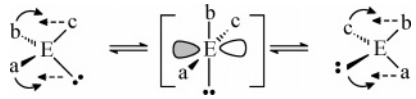

(i.e., inversion at these atoms via a mechanism involving Ge−N bond cleavage, Scheme 2), optimizations always converging to a transition state having a three-coordinate Ge center. Inversion at phosphorus via a transition state containing a trigonal planar P atom (**6a$_3$**) is calculated to have a moderate energy barrier of 21.0 kcal mol^{-1}. This is significantly lower than that calculated for PH_3 (35 kcal mol^{-1} at the MP2 level of theory); however, this value is consistent with previous NMR investigations on variously substituted phosphines which demonstrate that substitution of electropositive ER_3 groups (E = Si, Ge, Sn) around pyramidal phosphorus significantly reduces its inversion barrier.[25] For example, the inversion barrier for Ph*t*-Bu-MeP is 33.3 kcal mol^{-1} at 130 °C, whereas the inversion barriers for Ph*i*-Pr-P(SiMe$_3$) and Ph*i*-Pr-P(GeMe$_3$) are 18.9 (at 62 °C) and 21.4 kcal mol^{-1} (at 109 °C), respectively.

Attempts to find a trigonal planar transition state for inversion at germanium consistently converged to a transition state containing a T-shaped Ge center (**6a$_4$**) (Figure 7). This T-shaped transition state is some 38.5 kcal mol^{-1} higher in energy than the ground state (**6a$_1$**), a significant barrier to inversion at this center. The preference for a T-shaped rather than a trigonal planar transition state for inversion at germanium in **6a** is consistent with Dixon and Arduengo's previous calculations on the related, valence isoelectronic, pnictines and pnictine fluorides PnH_3 and PnF_3 (Pn = P, As, Sb).[26,27] These authors suggest that, whereas the PnH_3 compounds invert through a trigonal planar transition state (vertex inversion), the PnF_3 compounds invert through a T-shaped transition state (edge inversion, Scheme 4). The preference for edge inversion correlates with the electronegativity of the substituents at the pnictogen center: while PH_3 and PH_2F are calculated to undergo vertex inversion, both PHF_2 and PF_3 are predicted to undergo an edge-inversion process.[26a] Thus edge inversion at germanium in **6a** is consistent with the presence of an electronegative Cl substituent.

The phosphorus atom in transition state **6a$_4$** is essentially planar [sum of angles at P 359.98°] and the GePClN and $PGeC_2$ planes are closely aligned [angle between planes 17.38°]. Since the transition state in edge-inversion processes contains a vacant p-type orbital perpendicular to the molecular plane (Scheme 4),[27b] such transition states are likely to be stabilized by π-donor ligands (e.g., F, PR_2). Thus, in **6a$_4$** the planar P atom is

(25) Baechler, R. D.; Casey, J. P.; Cook, R. J.; Senkler, G. H., Jr.; Mislow, K. *J. Am. Chem. Soc.* **1972**, *94*, 2859.

(26) (a) Dixon, D. A.; Arduengo, A. J., III; Fukunaga, T. *J. Am. Chem. Soc.* **1986**, *108*, 2461. (b) Arduengo, A. J., III; Dixon, D. A.; Roe, D. C. *J. Am. Chem. Soc.* **1986**, *108*, 6821. (c) Dixon, R. A.; Arduengo, A. J., III. *J. Am. Chem. Soc.* **1987**, *109*, 338.

(27) (a) Schwerdtfeger, P.; Boyd, P. D. W.; Fischer, T.; Hunt, P.; Liddell, M. *J. Am. Chem. Soc.* **1994**, *116*, 9620. (b) Yamamoto, Y.; Chen. X.; Kojima, S.; Ohdoi, K.; Kitano, M.; Doi, Y.; Akiba, K. *J. Am. Chem. Soc.* **1995**, *117*, 3922. (c) Schwerdtfeger, P.; Laakkonen, L. J.; Pyykko, P. *J. Chem. Phys.* **1992**, *96*, 6807.

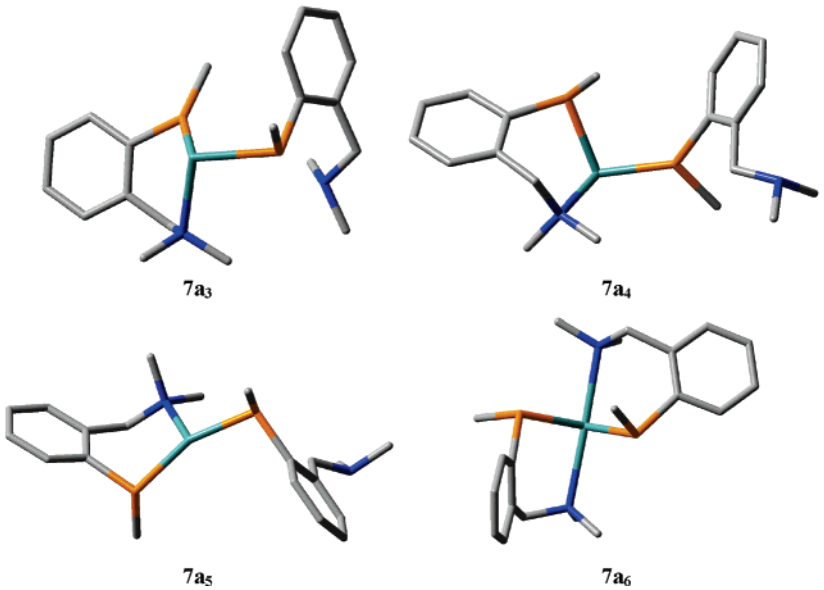

Figure 8. Transition states for inversion at the chelating (**7a$_3$**) and terminal (**7a$_4$**) phosphorus atoms and the germanium center (**7a$_5$**) and the calculated minimum for the trigonal bipyramidal intermediate in the Ge inversion process involving Ge−N coordination/scission (**7a$_6$**).

entirely consistent with an edge-inversion mechanism in which the p-type lone pair on phosphorus can overlap with the vacant p-type orbital on germanium.

Although slightly longer, the Ge−P and Ge−N distances in **6a$_4$** (2.477 and 2.323 Å, respectively) are within 0.06 Å of the corresponding distances calculated for **6a$_1$**; however, the Ge−Cl distance (2.524 Å) is more than 0.2 Å longer than the same distance in **6a$_1$**. The elongation of the Ge−X axial bonds is consistent with previous calculations on PHF_2 and PF_3 and related molecules, although the elongation of the equatorial Ge−N bond in **6a$_4$** is in marked contrast to the shortening of the equatorial Pn−F bonds observed in the edge-inversion transition states of PF_3 and AsF_3.[26a]

For compound **7a** transition states were found for inversion at either the P^{ch} (**7a$_3$**) or P^t (**7a$_4$**) centers with activation barriers of 24.0 and 18.5 kcal mol^{-1}, respectively (Figure 8). These inversion barriers compare well with the P inversion barrier calculated for **6a$_3$** (21.0 kcal mol^{-1}), and as expected, the inversion barrier for the terminal phosphide ligand is substantially lower than that for the chelating phosphide ligand.

In contrast to **6a** we were unable to find a transition state involving edge rather than vertex inversion at germanium for **7a**; this is consistent with the decreased electronegativity of the P^t atom in **7a** compared to the Cl substituent in **6a**. Inversion at germanium via a trigonal planar transition state (**7a$_5$**) was calculated to have a barrier of 48.5 kcal mol^{-1}, somewhat higher than the edge-inversion barrier of 38.5 kcal mol^{-1} calculated for **6a**, in line with Dixon and Arduengo's findings for the pnictine fluorides. For comparison, the barrier to edge inversion of AsF_3 is calculated to be 46.3 kcal mol^{-1} and the barrier to vertex inversion of AsH_3 is calculated to be 41.3 kcal mol^{-1} at the MP2 level of theory.[26a] In accord with previous observations, the Ge−P and Ge−N distances in **7a$_5$** are significantly shorter than those calculated for the starting geometry **7a$_1$**.

We were also unable to find a transition state for inversion at germanium via Ge−N cleavage/Ge−P rotation/Ge−N coordination (processes proceeding via **II** in Scheme 3). All attempts to find a saddle point corresponding to a two-coordinate germanium atom converged to give a four-coordinate, pseudo-trigonal bipyramidal germanium center (**7a$_6$**); this corresponds to the transition state for the associative mechanism for Ge inversion (**III**, Scheme 3). At the B3LYP level of theory this is calculated to be a minimum for **7a** rather than a transition state and is just 3.0 kcal mol^{-1} higher in energy than the lowest energy diastereomer **7a$_1$**. Of course, **7a** differs markedly from **7** in terms of the steric compression at the germanium and phosphorus centers, and this is likely to have a significant effect on the relative stability of such a transition state in the latter. However, convergence to **7a$_6$** suggests that an associative process may well play a part in the dynamic behavior observed for **7** in solution and that this process is likely to be significantly favored with respect to other Ge inversion processes.

Conclusions

The products of reactions between alkali metal derivatives of amino-functionalized phosphide ligands and germanium(II) halides are heavily dependent upon the alkali metal and the exact reaction stoichiometry. Reactions between $GeCl_2$ or GeI_2 and 2 equiv of the potassium phosphide **5** yield the diphosphagermylene **7**, whereas under the same conditions the reaction between 2 equiv of the lithium phosphide **4** yields the unusual ate complex **8**. Reactions between GeI_2 and 3 equiv of **5** yield the unusual ate cage complex **9**.

In solution the heteroleptic phosphagermylene **6** and the diphosphagermylene **7** are subject to dynamic equilibria which may be attributed to inversion processes at the Ge and/or P centers. Preliminary DFT calculations on the model complexes **6a** and **7a** suggest that these processes are most likely to involve inversion at P for **6a** but that, while inversion at the P centers may be accessible for **7a**, with inversion at the terminal P atom favored over inversion at the P atom in the chelating ligand, epimerization through inversion at the

Table 1. Crystallographic Data for 7, 8 and 9

	7	8	9
formula	$C_{32}H_{62}GeN_2P_2Si_4 \cdot 1/2C_7H_{14}$	$C_{32}H_{62}GeN_2P_2Si_4 \cdot Li_2I_2(C_4H_{10}O)_3$	$C_{48}H_{93}GeKN_3P_3Si_6$
fw	770.82	1211.77	1085.39
cryst size, mm	0.50 × 0.40 × 0.35	0.25 × 0.25 × 0.20	0.30 × 0.30 × 0.20
cryst syst	triclinic	orthorhombic	cubic
space group	$P\bar{1}$	$Pna2_1$	$Pa\bar{3}$
a, Å	11.4596(5)	48.748(3)	23.4873(5)
b, Å	12.0029(5)	11.2312(6)	
c, Å	16.3524(7)	11.1410(6)	
α, deg	78.569(1)		
β, deg	89.576(1)		
γ, deg	75.536(1)		
V, Å^3	2132.65(16)	6099.7(6)	12956.8(5)
Z	2	4	8
ρ_{calcd}, g cm^{-3}	1.200	1.320	1.113
μ, mm^{-1}	0.931	1.679	0.753
no. reflns measd	15612	49557	202438
no. unique reflns, R_{int}	9401, 0.0157	14270, 0.0481	4426, 0.0556
no. reflns with $F^2 > 2\sigma(F^2)$	8637	12469	3729
transmn coeff range	0.653−0.737	0.680−0.730	0.806−0.864
R, R_w[a] ($F^2 > 2\sigma$)	0.0268, 0.0755	0.0476, 0.0965	0.0402, 0.1185
R, R_w[a] (all data)	0.0299, 0.0776	0.0581, 0.0998	0.0548, 0.1358
absolute struct param		0.052(11)	
S[a]	1.036	1.106	1.167
refined params	413	561	195
max., min. diff map, e Å^{-3}	0.56, −0.53	0.72, −1.34	0.89, −0.29

[a] Conventional $R = \sum||F_o| - |F_c||/\sum|F_o|$; $R_w = [\sum w(F_o^2 - F_c^2)^2/\sum w(F_o^2)^2]^{1/2}$; $S = [\sum w(F_o^2 - F_c^2)^2/(\text{no. data} - \text{no. params})]^{1/2}$ for all data.

germanium center via a four-coordinate, pseudo-trigonal pyramidal transition state may be the lowest energy process. No evidence was found for inversion processes involving a two-coordinate germanium center.

The behavior of the amino-functionalized diphosphagermylene **7** and related compounds toward transition metal centers is currently under study.

Experimental Section

All manipulations were carried out using standard Schlenk techniques under an atmosphere of dry nitrogen or argon. Ether, THF, *n*-hexane, DME, methylcyclohexane, and light petroleum (bp 40−60 °C) were distilled under nitrogen from sodium, potassium, or sodium/potassium alloy; hexamethyldisiloxane was distilled under nitrogen from CaH_2. With the exception of THF, DME, and hexamethyldisiloxane, which were stored over activated 4 Å molecular sieves, all solvents were stored over a potassium film. Deuterated THF and toluene were distilled from potassium and deoxygenated by three freeze−pump−thaw cycles and were stored over activated 4 Å molecular sieves. All compounds were used as supplied by the manufacturer except the compounds $GeCl_2$(dioxane),[16] {R(C_6H_4-2-CH_2NMe_2)P}Li,[15a] and {R(C_6H_4-2-CH_2NMe_2)P}K,[15a] which were prepared by previously published methods.

^{1}H and ^{13}C NMR spectra were recorded on a JEOL Lambda 500 spectrometer operating at 500.16 and 125.65 MHz, respectively, or a Bruker Avance 300 spectrometer operating at 300.13 and 75.47 MHz, respectively; chemical shifts are quoted in ppm relative to tetramethylsilane. ^{31}P NMR spectra were recorded on a Bruker WM300 spectrometer operating at 121.5 MHz, and chemical shifts are quoted relative to external 85% H_3PO_4. The phase-sensitive ^{31}P EXSY spectrum was obtained at a measuring frequency of 202.47 MHz without proton decoupling and using a standard 90°−t_1−90°−τ_m−90°Acq(t_2) pulse sequence with 1024 data points in the t_2 dimension and 256 in t_1. Elemental analyses were obtained by the Elemental Analysis Service of London Metropolitan University.

Preparation of [{(Me$_3$Si)$_2$CH}(C$_6$H$_4$-2-CH$_2$NMe$_2$)P]GeCl (6). To a solution of $GeCl_2$(dioxane) (0.30 g, 1.295 mmol) in THF (10 mL) was added, dropwise, a solution of [{$(Me_3Si)_2CH$}(C_6H_4-2-CH_2NMe_2)P]K (0.47 g, 1.292 mmol) in THF (15 mL). This mixture was stirred for 16 h, and then solvent was removed in vacuo. The slightly sticky, colorless solid was extracted into hot hexamethyldisiloxane. This extract deposited colorless crystals of **6** on cooling. Yield: 0.91 g, 81%. Anal. Calcd for $C_{16}H_{31}ClGeNPSi_2$: C, 44.41; H, 7.24; N, 3.23. Found: C, 44.49; H, 6.69; N, 3.07. ^{1}H NMR (d_8-toluene, 297 K): δ 0.49 (s, 9H, $SiMe_3$), 0.60 (s, 9H, $SiMe_3$), 1.08 (d, $^2J_{PH}$ = 7.7 Hz, 1H, CHP), 1.72 (s, br, 3H NMe), 2.30 (s, br, 3H, NMe), ~2.9 (s, v br, 2H, CH_2N), 6.87−7.60 (m, 4H, ArH). ^{31}P{^{1}H} NMR (d_8-toluene 297 K): δ −34.9 (br s).

Preparation of [{(Me$_3$Si)$_2$CH}(C$_6$H$_4$-2-CH$_2$NMe$_2$)P]$_2$Ge (7). To a suspension of GeI_2 (0.73 g, 2.236 mmol) in THF (20 mL) was added, dropwise, a solution of [{$(Me_3Si)_2CH$}(C_6H_4-2-CH_2NMe_2)P]K (1.27 g, 3.891 mmol) in THF (40 mL). This mixture was allowed to stir for 16 h, and then solvent was removed in vacuo. The sticky yellow solid was extracted into light petroleum and filtered. Solvent was removed in vacuo from the filtrate, and the sticky solid was recrystallized from cold (−30 °C) hexamethyldisiloxane containing a few drops of DME as yellow blocks of **7**. Yield: 1.13 g, 70%. Anal. Calcd for $C_{32}H_{62}GeN_2P_2Si_4$: C, 52.25; H, 8.66; N, 3.88. Found: C, 52.95; H, 8.67; N, 3.96. ^{1}H NMR (d_8-toluene, 363 K): δ 0.22 (s, 36H, $SiMe_3$), 0.53 (s, 2H, CHP), 2.09 (s, 12H, NMe_2), 3.58 (s, 4H, CH_2N), 6.91−7.80 (m, 8H, ArH). ^{31}P{^{1}H} (d_8-toluene, 363 K): δ −45.8.

Preparation of [{(Me$_3$Si)$_2$CH}(C$_6$H$_4$-2-CH$_2$NMe$_2$)P]$_2$-GeLi$_2$I$_2$(OEt$_2$)$_3$ (8). To a suspension of GeI_2 (0.46 g, 1.409 mmol) in cold (−78 °C) ether (10 mL) was added, dropwise, a solution of [{$(Me_3Si)_2CH$}(C_6H_4-2-CH_2NMe_2)P]Li (0.93 g, 2.818 mmol) in ether (10 mL). This mixture was allowed to attain room temperature and was stirred for 12 h. Solvent was removed in vacuo, and the residue was extracted into methylcyclohexane (20 mL) and filtered. The filtrate was concentrated to ca. 5 mL and was cooled to −30 °C for 12 h, after which time pale yellow crystals of **8** were isolated and washed with a little cold petroleum ether. Yield: 1.08 g 63%. Anal. Calcd for $C_{44}H_{92}GeI_2Li_2N_2O_3P_2Si_4$: C, 43.61; H, 7.65; N, 2.31. Found: C, 43.72; H, 7.79; N, 2.20. ^{1}H NMR (d_8-THF, 298 K): δ 0.01 (s, br, 18H, $SiMe_3$), 0.08 (s, br, 18H, $SiMe_3$), 0.17 (s, br, 2H, CHP), 1.08 (t, 18H, Et_2O), 2.27 (s, br, 12H, NMe_2), 3.37

(q, 12H, Et_2O), 3.68 (s, br, 2H, CH_2N), 3.81 (s, br, 2H, CH_2N), 7.04−7.75 (m, 8H, ArH). $^{31}P\{^1H\}$ NMR (d_8-THF, 333 K): δ −48.1.

Preparation of [{(Me$_3$Si)$_2$CH}(C$_6$H$_4$-2-CH$_2$NMe$_2$)P]$_3$GeK (9). To a solution of $GeCl_2$(dioxane) (0.15 g, 0.648 mmol) in THF (5 mL) was added a solution of [{$(Me_3Si)_2CH$}(C_6H_4-2-CH_2NMe_2)P]K (0.69 g, 1.897 mmol) in THF (10 mL). This mixture was stirred for 12 h, and then solvent was removed in vacuo. The sticky solid was extracted into *n*-hexane and filtered. The filtrate was concentrated to ca. 5 mL and cooled to −30 °C for 12 h. Deep red crystals of **9** were isolated and washed with a little cold light petroleum. Yield: 0.38 g, 54%. Anal. Calcd for $C_{48}H_{93}GeKN_3P_3Si_6$: C, 53.11; H, 8.64; N, 3.87. Found: C, 52.99; H, 8.54; N, 3.82. ^1H NMR (d_8-toluene, 297 K): δ 0.24 (s, 27H, $SiMe_3$), 0.96 (s, 27H, $SiMe_3$), 2.48 (s, 18H, NMe_2), 3.05 (d, J_{HH} = 11.3 Hz, 3H CH_2N), 5.08 (d, J_{HH} = 11.3 Hz, 3H, CH_2N), 7.36−8.91 (m, 12H, ArH). $^{31}P\{^1H\}$ NMR (d_8-toluene, 297 K): δ −55.3.

Crystal Structure Determinations of 7, 8, and 9. For **7**, **8**, and **9** measurements were made at 150 K on a Bruker AXS SMART CCD diffractometer using graphite-monochromated Mo Kα radiation (λ = 0.71073 Å) and narrow (0.3° in ω) frame exposures. For all compounds cell parameters were refined from the observed positions of all strong reflections in each data set. Intensities were corrected semiempirically for absorption, based on symmetry-equivalent and repeated reflections. The structures were solved by direct methods and refined on F^2 values for all unique data. Table 1 gives further details. All non-hydrogen atoms were refined anisotropically, and H atoms were constrained with a riding model; U(H) was set at 1.2 (1.5 for methyl groups) times U_{eq} for the parent atom. Programs were Bruker AXS SMART (control) and SAINT (integration), and SHELXTL for structure solution, refinement, and molecular graphics.[28]

DFT Calculations. Geometry optimizations on the gas-phase molecules were performed with the GAMESS(US) program[29] on an SGI Affix 3700 computer. Initial optimizations were performed using the B3LYP hybrid functional[22] with an SBKJC effective core potential basis set for all atoms.[23] The calculated geometries were then reoptimized using all-electron basis sets, 6-311G* on the Ge, N, and P atoms and 3-21G* on the C and H atoms [default parameters were used throughout].[24] Minima were confirmed by the absence of imaginary vibrational frequencies and transition states by the presence of a single imaginary vibrational frequency.

Acknowledgment. The authors are grateful to the Royal Society for support. Prof A. Harriman is thanked for his assistance with the DFT calculations.

Supporting Information Available: For **7**, **8**, and **9** details of structure determination, atomic coordinates, bond lengths and angles, and displacement parameters in CIF format. For **6a** and **7a** details of DFT calculations, final atomic coordinates (in both text and PDB format), and energies. Complete details of ref 29. This material is available free of charge via the Internet at http://pubs.acs.org. Observed and calculated structure factor details are available from the authors upon request.

OM0501125

(28) (a) *SMART* and *SAINT* software for CCD diffractometers; Bruker AXS Inc.: Madison, WI, 1997. (b) Sheldrick, G. M. *SHELXTL* user manual, version 6; Bruker AXS Inc.: Madison, WI, 2001.

(29) Schmidt, M. W.; et al. *J. Comput. Chem.* **1993**, *14*, 1347.